Synthesis, XRD single crystal structure analysis, vibrational spectral analysis, molecular dynamics and molecular docking studies of 2-(3-methoxy-4-hydroxyphenyl) benzothiazole

Article title: Synthesis, XRD single crystal structure analysis, vibrational spectral analysis, molecular dynamics and molecular docking studies of 2-(3-methoxy-4-hydroxyphenyl) benzothiazole

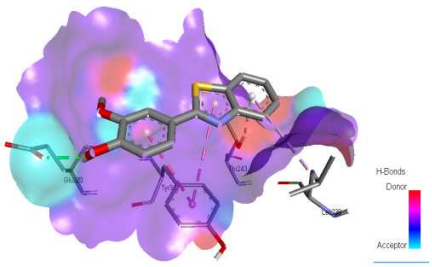

Synthesis, XRD single crystal structure analysis, vibrational spectral analysis, molecular dynamics and molecular docking studies of 2-(3-methoxy-4-hydroxyphenyl) benzothiazole

A.Sarau Devi[a], V.V.Aswathy[b], Y.Sheena Mary[b]*, C.Yohannan Panicker[b], Stevan Armaković[c], Sanja J. Armaković[d], Reena Ravindran[e], C.Van Alsenoy[f]

[a]Department of Chemistry, Fatima Mata National College, Kollam, Kerala, India
[b]Department of Physics, Fatima Mata National College, Kollam, Kerala, India
[c]University of Novi Sad, Faculty of Sciences, Department of Physics,
Trg D. Obradovića 4, 21000 Novi Sad, Serbia
[d]University of Novi Sad, Faculty of Sciences, Department of Chemistry, Biochemistry and Environmental Protection, Trg D. Obradovića 3, 21000 Novi Sad, Serbia
[e]Department of Chemistry, Sree Narayana College, Chempazhanthy, Thiruvananthapuram, Kerala, India
[f]Department of Chemistry, University of Antwerp, Groenenborgerlaan 171, B-2020, Antwerp, Belgium
*author for correspondence: email: sypanicker@rediffmail.com

Abstract

The vibrational spectra and corresponding vibrational assignments of 2-(3-methoxy-4-hydroxyphenyl)benzothiazole is reported. Single crystal XRD data of the title compound is reported and the orientation of methoxy group is *cis* to nitrogen atom of the thiazole ring. The phenyl ring breathing modes of the title compound are assigned at 1042 and 731 cm^{-1} theoretically. The charge transfer within the molecule is studied using frontier molecular orbital analysis. The chemical reactivity descriptors are calculated theoretically. The NMR spectral data predicted theoretically are in good agreement with the experimental data. The strong negative region spread over the phenyl rings, nitrogen atom and oxygen atom of the hydroxyl group in the MEP plot is due to the immense conjugative and hyper conjugative resonance charge delocalization of π-electrons. Molecule sites prone to electrophilic attacks have been determined by analysis of ALIE surfaces, while Fukui functions provided further insight into the local reactivity properties of title molecule. Autoxidation properties have been investigated by calculation of bond dissociation energies (BDEs) of hydrogen abstraction, while BDEs of the rest of the single acyclic bonds were valuable for the further investigation of degradation properties. Calculation of radial distribution functions was performed in order to determine which atoms of the title molecule have pronounced interactions with water

molecules. The title compound forms a stable complex with aryl hydrocarbon receptor and can be a lead compound for developing new anti-tumor drug. Antimicrobial properties of the title compound was screened against one bacterial culture *Escherchia coli* and four fungal cultures *viz*., *Aspergillus niger*, *Pencillum chrysogenum*, *Saccharomyces cerevisiae* and *Rhyzopus stolonifer*.

Keywords: DFT; Thiazole; ALIE; RDF; BDE; molecular docking.

1. Introduction

Benzothiazole derivatives are of biologically active heterocyclics with luminescence property. It is used as a starting material for synthesis of larger, usually bioactive structures. 2-substituted benzothiazoles are now of great interest due to their pharmacological and optical activities. The luciferase enzyme used in nature for bioluminescence is constituted by benzothiazole fragments. Some benzothiazole derivatives and its complexes belong to a class of organic luminescent materials, which are used as fluorescent brighteners as well as in organic light emitting diodes [1-3]. Furthermore they attracted attention as two-photon absorption chromophores, liquid crystals, photo conducting materials and flurophores [4-6]. Incorporation of a thiazole subunit into large delocalized π-electron systems enhances the hyperpolarizability and good candidates for the display of large non-linear responses and hence benzothiazoles are excellent nonlinear optical chromophores [7, 8]. The pharmacological activity includes antitumor, antifungal, antioxidant and photo sensitizing properties [9-12]. These compounds may be useful as fluorescent tracers for detecting β-amyloid in Alzheimer's brains [13]. The vibrational spectroscopic studies of certain phenothiazine derivatives are reported by the authors group [14, 15].

Scientific community is strongly devoted to the investigation of economic and efficient degradation mechanisms for the pharmaceutical products based on biologically active molecules. Namely, this type of the compounds has been slowly entering environment and represents great threat to the aquatic organisms. So far pharmaceuticals have been detected in all types of water [16-18], while conventional purification procedures are not adequate for their removal. In this regard advanced oxidation processes are seen as alternative approaches for improved degradation of mentioned class of compounds [19-21].

Detailed investigation of degradation properties of some molecule is time consuming and tedious procedure in which all degradation intermediates should be detected and confirmed. Herein, DFT calculations coupled with molecular dynamics simulations are of great help because they enable one to obtain initial information on the degradation properties by relatively inexpensive computational experiments. Concretely, two aspects of degradation

can be initially assessed by mentioned computational experiments; by calculation of bond dissociation energies one is able to predict where the process of autoxidation could happen, while MD simulations allow one to see which molecule atoms are under significant influence of solvent molecules (most frequently water molecules). In this work we have been calculated BDEs for all single acyclic bonds and calculated radial distribution functions after MD simulations in order to investigated the oxidative and hydrolysis aspects of degradation of the title molecule [22,23].

2. Experimental details

2.1 Synthesis of benzothiazole ligand

Equimolar mixture of $NaHSO_3$ (1.25 g, 0.012 M) and vanillin (1.82 g, 0.012 M) were refluxed in ethanol (15 mL) for 15-20 minutes. To the mixture o-aminothiophenol (1.25 g, 0.01 M) was added and continued to reflux for 4-5 h. On slow cooling, colorless crystalline compound formed was filtered, washed with water, re-crystallized from ethanol and dried over fused $CaCl_2$. M.P. 171ºC. The solution state spectrum in methanol was recorded on a Spectro UV-Vis Double Beam UVD-3500 spectrometer. Infrared spectrum (Fig.S1-supporting material) was recorded on a Thermo Nicolet AVATAR 370 DTGS model FT-IR spectrophotometer in the range 4000-400 cm^{-1} using KBr pellets. The FT-Raman spectrum (Fig.S2-supporting material) was recorded on a Bruker RFs 100/s, Germany, with an excitation wave length 1064 nm.

2.2 DART-mass spectral studies

DART-MS spectrum (Fig.S3-supporting material) [24] of the compound was recorded on a JEOL-AccuTOF DART JMS-TI00LC mass spectrometer having TOF mass analyzer and DART (Direct Analysis in Real Time) source at the Central Drug Research Institute, Lucknow, India. The molecular ion peak is observed at m/z 258.08 and $[M+H]^+$ as a less intense peak at m/z 259.08.

2.3. Crystal structure

The title compound (ORTEP diagram Fig.S4-supporting material) crystallizes into an orthorhombic lattice with space group $P2_12_12_1$. In the thiazole ring of benzothiazole, the C_{11}-N_{25} bond length of 1.297(2) Å is similar to that of typical C=N bond. The other bond lengths are intermediate between ideal values of corresponding single and double bonds giving evidence for extended π-delocalization throughout the entire molecule [25]. The molecule as a whole adopt almost planar conformation but for the slight tilt of vanillyl ring as evidenced by the torsion angle of -4.7(2)° corresponding to the N_{25}-C_{11}-C_{12}-C_{19} plane and -4.1(3)° corresponding to the S_{28}-C_{11}-C_{12}-C_{19} plane. The torsion angles S_{28}-C_{11}-C_{12}-C_{19} and N_{25}-C_{11}-

C_{12}-C_{13} have values of 176.15(13)° and 175.01(17)° respectively. The orientation of methoxy group is cis to N_{25} of thiazole ring. The unit cell packing of the title compound viewed down 'a and b' axis is shown in Fig.S5(supporting material).

The unit cell of the crystal consists of a set of four molecules held together by hydrogen bonding involving O_{27}-H_{29}…N_{25} forming a zig-zag chain, which forms the repeating unit of the packing in the crystal lattice. In addition to hydrogen bonding there is a bifurcated interaction between C_{19}-H_{20} of one molecule with O_{27} (2.432Å) and H_{29}-O_{27} (2.194Å). The assemblage of molecules *via* O–H…N hydrogen bonding, C-H…O short contact and C-H…π interaction constitute supra-molecular net work. The overall packing in two-dimension is affected by the offset alignment of neighboring layers by a weak C-H…π interaction between C_{15}…$H_{22,23,24}$ (2.795 Å). Details of the data collection conditions and the parameters of the refinement process of 2-(3-methoxy-4-hydroxyphenyl)benzothiazole are given in Table S1 (supporting material).

2.4 Fluorescent Properties

It has been proved that benzothiazoles exhibit strong luminescence in solution and in solid state, due to the presence of electron-withdrawing hetero aromatic ring incorporating with the π-conjugated system and electron donating chromophores [3, 26]. The emission spectrum measured in methanolic solution at 298K is characterized by a broad band centered at 408 nm, upon excitation at 285 nm.

3. Computational details

The molecular geometry optimization, hyperpolarizabilities, NBO analysis [27] for the isolated gas phase of the title compound in the ground state are calculated by the density functional using B3LYP/6-311++G(d) (5D, 7F) [28] level of theory using Gaussian09 software [29]. The vibrational assignments were carried out on the basis of potential energy distribution analysis using GAR2PED program [30] and with the aid of Gaussview software [31]. A scaling factor of 0.9613 [32] is uniformly applied for the calculated theoretical wave numbers. The optimized geometrical parameters (Fig.1) of the title compound with XRD data are given in Table S2 (supporting material).

Average local ionization energies (ALIE) have been calculated and mapped to the electron density surfaces using the Jaguar 9.0 [33] program, as implemented in Schrödinger Materials Science Suite 2015-4 [34]. Same program was used for the calculation of Fukui functions and bond dissociation energies (BDE) of all single acyclic bonds. In all DFT calculations performed with Jaguar a B3LYP [35] exchange-correlation functional has been used with 6-311++G(d,p) basis set for ALIE surface, 6-31+G(d) for Fukui functions and 6-

311G(d,p) for BDEs. Radial distribution functions (RDF) have been calculated after MD simulations performed with Desmond [36-39] program, also as implemented in Schrödinger Materials Science Suite 2015-4. OPLS 2005 force field [40] with NPT ensemble class were used with pressure set to 1.0325 bar and temperature to 300 K. Simulation time was 5 ns with cut-off radius of 12 Å. NVT ensemble class was used in the first 100 ps of simulation in order to relax the system. Modeled system consisted of one title molecule in cubic box with ~3000 water molecules, where solvent was treated with simple point charge (SPC) model [41]. To detect and investigate intramolecular noncovalent interactionsthe method of Johnson was used [42, 43].

4. Results and discussion

In the following discussions, tri-substituted and 1,2-substituted phenyl rings and thiazole rings are designated as PhI, PhII and PhIII, respectively.

4.1 Geometrical parameters

The C-C bond lengths (DFT/XRD) in the phenyl rings lie in the ranges 1.4105-1.3828/1.4023-1.3793Å for PhI and 1.4139-1.3878/1.4003-1.3753Å for PhII whereas the C-C bond length for benzene is 1.3993Å [44]. For the title compound, the C-O bond lengths (DFT/XRD) are C_{17}-O_{27} = 1.3574/1.3492Å, C_{18}-O_{26} = 1.3718/1.3622Å and C_{21}-O_{26} = 1.4233/1.4133Å which are in agreement with reported values [45]. The C-S bond lengths (DFT/XRD) of the title compound are 1.7894/1.7512Å and 1.7502/1.7332Å while the reported values are 1.7822/1.7602Å, 1.7782/1.7535Å [46] and 1.7627/1.7380Å, 1.7799/1.7385Å [47]. The C=N bond lengths (DFT/XRD) of the title compound are 1.2972/1.2972Å and 1.3803/1.3872Å which are in agreement with literature [14, 15].

The bond angles (DFT/XRD) at C_{11} and C_{12} positions are respectively, C_{12}-C_{11}-N_{25} = 124.2/1.24.7°, C_{12}-C_{11}-S_{28} = 121.3/120.2°, N_{25}-C_{11}-S_{28} = 114.6/115.2° and C_{13}-C_{12}-C_{11} = 122.6/122.1°, C_{13}-C_{12}-C_{19} = 119.1/119.2°, C_{19}-C_{12}-C_{11} = 118.4/119.0° and this reveals the interaction between the phenyl rings and the thiazole group. Similarly at C_{18} position the bond angles (DFT/XRD) are C_{17}-C_{18}-C_{19} = 120.4/120.2°, C17-C18-O_{26} = 113.7/114.6° and C_{19}-C_{18}-O_{26} = 125.9/125.2° and this asymmetry in angles reveal the hydrogen bonding between the OH group and methoxy group. The torsion angles between the phenyl rings and thiazole are nearly 180.0° which show the thiazole ring is planar with respect to the phenyl rings.

4.2 IR and Raman spectra

The calculated scaled wave numbers, observed IR bands and assignments of the title compound are given in Table 1.

According to literature, the C-O-C stretching modes are expected in the region 1200-850 cm^{-1} [48, 49]. As expected, the C-O-C stretching modes are assigned at 1144, 1018 cm^{-1} theoretically for the title compound and experimentally bands are observed in the IR spectrum at 1015 cm^{-1} and 1019 cm^{-1} in the Raman spectrum which are in agreement with the literature [50]. El-Azab et al. [51] reported the C-O-C stretching vibrations at 951 cm^{-1} in the IR spectrum, 1201, 980, 915 cm^{-1} in the Raman spectrum and at 1198, 1009, 978, 948, 911, 848 cm^{-1} theoretically for tri-methoxy phenyl derivatives. The CH_3 vibrations of the methoxy group are expected in the ranges, 3050-2900 cm^{-1} (stretching modes), 1500-1400 cm^{-1} and 1200-1100 cm^{-1} (deformation modes) [48, 52] and in the present case these modes are assigned at 3027, 2970, 2908 cm^{-1} (stretching) and 1460, 1450, 1437, 1185, 1136 cm^{-1} (deformation modes) theoretically. Experimentally the bands observed at 3002, 2972, 2920 cm^{-1} (stretching) and 1458, 1190 cm^{-1} (deformation) in the IR spectrum and at 3003, 2970, 2905 cm^{-1} (stretching) and 1190, 1132 cm^{-1} (deformation) are assigned as the CH_3 stretching and deformation modes.

The OH stretching vibration is expected in the range 3380 ± 200 cm^{-1} [48] and for the title compound the O-H stretching vibration is assigned at 3587 cm^{-1} theoretically. The in-plane OH deformation mode is assigned at 1361 cm^{-1} in the IR spectrum, 1362 cm^{-1} in the Raman spectrum and at 1359 cm^{-1} theoretically for the title compound which is expected in the range 1400-1480 cm^{-1} [48]. The C-O stretching mode of the hydroxyl group of the title compound is assigned at 1229 cm^{-1} theoretically which is expected in the range 1180-1260 cm^{-1} [48, 50, 52, 53]. Benzon et al. [54] reported the OH deformation mode at 1406 cm^{-1} and C-O stretching mode at 1212 (IR), 1228 (Raman) and at 1229 cm^{-1} theoretically for hydroxyl group.

For the title compound, the PED analysis gives the C=N stretching mode at 1467 cm^{-1} and C-N stretching mode at 1219 cm^{-1} theoretically as expected [48] and Benzon et al. [54] reported value this mode at 1515 cm^{-1} in the IR spectrum, 1520 cm^{-1} in the Raman spectrum, 1517 cm^{-1} theoretically. The C-S stretching modes of the title compound are assigned at 759, 660 cm^{-1} theoretically and experimentally bands are observed at 756, 665 cm^{-1} in the IR spectrum and at 756, 658 cm^{-1} in the Raman spectrum as expected [48]. The reported values of the CS stretching vibrations are 770, 663 cm^{-1} (DFT) and 770 cm^{-1} (IR) [51].

For phenyl derivatives, the C-H stretching modes are expected above 3000 cm^{-1} [48] and PED analysis gives the C-H stretching modes at 3098, 3075, 3055 cm^{-1} for PhI and at 3072, 3066, 3055, 3044 cm^{-1} for PhII. Experimentally these modes are observed at 3096 cm^{-1} in the IR spectrum and at 3097, 3063, 3038 cm^{-1} in the Raman spectrum. Phenyl ring

stretching modes are assigned at 1585, 1361 cm^{-1} (IR), 1585 cm^{-1} (Raman), 1583, 1579, 1406, 1359, 1261 cm^{-1} (DFT) for PhI and at 1533, 1420, 1293 cm^{-1} (IR), 1565, 1532, 1434, 1420, 1301 cm^{-1} (Raman), 1569, 1537, 1433, 1412, 1295 cm^{-1} (DFT) for PhII, as expected in literature [48, 53]. In ortho-di-substitution the ring breathing mode of the phenyl ring has three frequency intervals, 1100-1130 cm^{-1} (both substituent are heavy), 1020-1070 cm^{-1} (one of them is heavy while the other is light) 630-780 cm^{-1} (both of them are light) [53]. In the present case, the ring breathing mode of the ring PhII is assigned at 1044 cm^{-1} in the IR spectrum, 1038 cm^{-1} in the Raman spectrum and at 1042 cm^{-1} theoretically as expected [48, 53]. For ortho substituted phenyl ring the ring breathing mode is reported at 1041 cm^{-1} [55] and at 1086, 1011 cm^{-1} theoretically [56] and at 1020 cm^{-1} theoretically [57]. In the case of tri-substituted benzenes, with mixed substituent, the ring breathing mode is expected in the range 600-750 cm^{-1} [53] and in the present case, the PED analysis give the ring breathing mode at 731 cm^{-1} (DFT) for the tri-substituted phenyl ring and a band is observed in the Raman spectrum at 729 cm^{-1}. The ring breathing mode of tri-substituted phenyl ring is reported at 738 cm^{-1} by Mary et al. [58] and at 742 cm^{-1} by Panicker et al. [59]. The in-plane CH bending modes of the phenyl rings are assigned theoretically at 1277, 1170, 1108 cm^{-1} for PhI ring and at 1248, 1140, 1102, 1042 cm^{-1} for PhII ring, which are expected above 1000 cm^{-1} [48] and experimentally bands are observed at 1250, 1114, 1044 cm^{-1} in the IR spectrum and 1279, 1246, 1168, 1038 cm^{-1} in the Raman spectrum. The out-of-plane CH bending modes are assigned theoretically at 895, 858, 790 cm^{-1} for PhI and at 930, 897, 818, 731 cm^{-1} for PhII as expected [48]. The corresponding experimental IR bands are 931, 896, 855 and 816 cm^{-1} and Raman bands are 788, 729 cm^{-1}. The ring in-plane and out-of-plane deformation modes are also identified and assigned (Table 1) and most of the modes are not pure, but contains significant contributions from other modes also.

4.3 NMR spectra

The absolute isotropic chemical shielding was calculated by B3LYP/GIAO model [60] and relative chemical shifts were then estimated by using the corresponding TMS shielding: σ_{calc} (TMS) calculated in advance at the same theoretical level as this paper and numerical values of chemical shift $\delta_{calc} = \sigma_{calc}(TMS) - \sigma_{calc}$ together with calculated values of $\sigma_{calc}(TMS)$, are given in Table S3 (supporting material). The protons of the phenyl rings I and II resonate in the ranges, 8.2669-7.2017 ppm and 8.2106-7.7007 ppm theoretically and 6.99-7.72 and 7.35-8.03 ppm experimentally [61]. The circulation of the double bond electrons in a secondary magnetic field accounts for the formation of magnetic anisotropy. Therefore, predicted chemical shifts of the hydrogen atoms of the CH_3 groups are 4.3016, 4.4693,

4.3017 ppm while the experimental shift is 4.08 ppm. The chemical shifts of the hydrogen atom with the hydroxyl OH is 5.6147 (predicted) and 6.05 ppm (experimentally). The $–OCH_3$ protons show a slight downward shift to 4.08 ppm due to the withdrawal of electron density by adjacent OH group [62]. The OH peak of the title compound is observed at 6.05 ppm. Due to the combined resonance and inductive effect of -OH and $-OCH_3$ groups in the title compound, H20 peak is observed as a singlet at 7.72 ppm and H16 and H14 are observed as doublets at 7.53 and 6.99 ppm, respectively.

For aromatic carbon atoms, the range of ^{13}C NMR shifts are normally greater than 100 ppm [63, 64] and for the title compound, ^{13}C NMR chemical shifts of the entire phenyl carbon atoms are greater than 100 ppm as expected in literature. The predicted shifts lie in the ranges 148.2968-109.9095 ppm for PhI ring and 151.9663-121.4295 ppm for PhII ring. The corresponding experimental values are 154.09-109.29 for PhI and 146.95-121.52 ppm for PhII. The predicted chemical shift of carbon atom in the CH_3 group is 59.6262 ppm and in the thiazole group is 171.2414 ppm while the experimental values are 56.21 and 168.13 ppm. For the carbon atoms, C_{11} the high chemical shift is due to the neighboring nitrogen and sulfur atoms.The ^{13}C NMR spectra provide direct information about the carbon skeleton of the molecule. The thiazolyl carbon atom C11 resonate 168.13 ppm. This is due to the conjugative effect of adjacent N and S of benzothiazole moiety. The C17 of the title compound resonate at a lower field at 154.09 ppm due to the influence of OH group and C18 resonate at 148.53 due to the presence of OCH_3 group.

4.4 Natural Bond Orbital analysis

The important hyper-conjugative interactions are: C_{11}-S_{28} from N_{25} of $n_1(N_{25})\rightarrow \sigma^*(C_{11}\text{-}S_{28})$, C_{18}-C_{19} from O_{26} of $n_2(O_{26})\rightarrow\pi^*(C_{18}\text{-}C_{19})$, C_{15}-C_{17} from O_{27} of $n_2(O_{27})\rightarrow \pi^*(C_{15}\text{-}C_{17})$ and C_{11}-N_{25} from S_{28} of $n_2(S_{28})\rightarrow\pi^*(C_{11}\text{-}N_{25})$ with electron densities, 0.11002, 0.35686, 0.02096, 0.33010e and stabilization energies, 19.61, 24.24, 26.97 and 20.88 kJ/mol.

The NBO analysis also describes the bonding in terms of the natural hybrid orbital; the orbital with higher energies, 100% p-character, low occupation number are: $n_2(O_{26})$, $n_2(O_{27})$ and $n_2(S_{28})$ with energies, -0.32812, -0.31776 and -0.25532a.u and occupation numbers, 1.87549, 1.86681 and 1.72982. While the orbital with lower energies, high occupation numbers are: $n_1(O_{26})$, $n_1(O_{27})$ and $n_1(S_{28})$ with energies, -0.56899, -0.574104 and -0.66221a.u. and p-characters, 57.87, 54.24 and 31.86% and occupation numbers, 1.96151, 1.97859 and 1.98027. Thus, a very close to pure p-type lone pair orbital participates in the electron donation to the $n_1(N_{25})\rightarrow\sigma^*(C_{11}\text{-}S_{28})$, $n_2(O_{26})\rightarrow\pi^*(C_{18}\text{-}C_{19})$, $n_2(O_{27})\rightarrow\pi^*(C_{15}\text{-}C_{17})$,

and $n_2(S_{28})\rightarrow\pi^*(C_{11}\text{-}N_{25})$ interactions in the compound. The results are tabulated in Tables S4 and S5 (supporting material).

4.5 Electronic absorption spectrum

In order to understand the electronic transitions of 2-(3-methoxy-4-hydroxyphenyl)benzothiazole, TD-DFT calculation on electronic absorption spectrum in vacuum was performed. The absorption spectra of organic compounds stem from the ground-to-excited state vibrational transition of electrons. The intense band in the UV range of the electronic absorption spectrum is observed at 318 nm, which is indicating the presence of chromophoric $–OCH_3$ and auxochromic –OH entity in the compound. The calculated seven lowest-energy transitions of the molecule from TD-DFT method and the observed electronic transitions are listed in Table 2. While in the experimental UV spectrum, the bands due to π-π* transitions of benzo chromophore are observed at 220 nm and at 285 nm assigned to π-π* transition of substituted phenyl ring and the long wavelength (> 300 nm) band observed at 328 nm has been attributed to n-π* transitions of thiazole ring and OH chromophore.

4.6 Nonlinear Optical properties

The use of organic materials in optoelectronics has increased dramatically and the increasing volume of information processing and communication in continuing to be a big challenge in the modern technology [65]. To find the nonlinear optical response of the title compound, the nonlinear optical parameters such as polarizability, the first and second order hyperpolarizability of the title compound are calculated using B3LYP/6-31G(d,p) (6D, 7F) basis set level. For the title compound, polarizability and first hyperpolarizability are 3.234×10^{-23} esu and 19.674×10^{-30} esu and the first hyperpolarizability is 151.34 times that of the standard NLO material urea [66] and the first hyperpolarizability is comparable with that of similar derivatives [14,15]. Second hyperpolarizability of the title compound is calculated by using the equation $\gamma_{av}= 1/5[\gamma_{xxxx} + \gamma_{yyyy} + \gamma_{zzzz} + 2\gamma_{xxyy} + 2\gamma_{xxzz} + 2\gamma_{yyzz}]$ and the value is -13.986×10^{-37} esu.

4.7 Frontier molecular orbital analysis

The highest occupied molecular orbital and the lowest unoccupied molecular orbital plot of the title compound calculated at the B3LYP/6-311++G(d) (5D, 7F) is given in Fig.S6 (supporting material). HOMO and LUMO and their properties are used to explain several types of reactions and for predicting the most reactive position in conjugated systems [67].The energy values of HOMO and LUMO and the energy gap reflect the biological activity of a molecule and a molecule having a small energy gap is more polarisable and is

generally associated with a high chemical reactivity and low kinetic stability [68, 69]. HOMO is the outer orbital containing electrons and tends to give these electrons as an electron donor and hence the ionization potential is directly related to the energy of the HOMO while the LUMO can accept electrons and the LUMO energy is directly related to electron affinity [70, 71]. From Fig.S6, the HOMO-LUMO plot, it is very clear that the HOMO is localized over the entire molecule except the methoxy group, while the LUMO is over the entire molecule except the methyl group and there is a possibility of charge transfer in the system through these regions. For the title compound, E_{HOMO} = -7.885 eV, E_{LUMO} = -5.168 eV and the HOMO-LUMO energy gap = 2.717 eV. Ionization potential, I, electron affinity, A, electronegativity, χ, global hardness, η, chemical potential, μ and global electrophilicity index, ω, [72] were calculated using the equations, I= $-E_{HOMO}$ = 7.885, A= $-E_{LUMO}$ = 5.168, $\chi = -(E_{HOMO}+E_{LUMO})/2$ = 6.5265 eV, η= =(I-A)/2 = 1.3585 eV, $\mu = -(I+A)/2$ = -6.5265 eV and $\omega = \mu^2/2\eta$ = 15.677 eV.

4.8 Molecular Electrostatic Potential surface

The iso-surfaces of the electrostatic potential are generated at B3LYP/6-311++G(d) (5D, 7F) level of theory is mapped onto the total electron density of the molecule and is depicted in Fig. S7 (supporting material). Molecular electrostatic potential surface of the title compound has strong negative region spread over the phenyl rings, nitrogen atom and oxygen atom of the hydroxyl group due to the immense conjugative and hyper conjugative resonance charge delocalization of π-electrons. All the unperturbed hydrogen atoms are associated with positive electrostatic potential especially the hydrogen atom of the hydroxyl group.

4.9 ALIE surfaces, non-covalent interactions and Fukui functions

To determine which molecule areas are prone to electrophilic attacks it is better to use ALIE than MEP surfaces. In particular, ALIE shows the locations where electrons are least tightly bound and therefore most easily removed. This important quantum molecular descriptor is defined as sum defined as a sum of orbital energies weighted by the orbital densities [43, 73]:

$$I(r) = \sum_i \frac{\rho_i(\vec{r})|\varepsilon_i|}{\rho(\vec{r})}, \qquad (1)$$

where $\rho_i(\vec{r})$ represents the electronic density of the *i*-th molecular orbital at the point $\vec{r}$, ε_i represents the orbital energy and $\rho(\vec{r})$ is the total electronic density function. ALIE is the most useful when its values are mapped to the electron density surface, Fig.2.

It can be seen in Fig.2 that red color is significantly distributed over the whole title molecule. Beside benzene rings, red color is located in the near vicinity of nitrogen atom N25 and sulfur atom S28, designating these atoms as possibly prone to electrophilic attacks. Beside these, near vicinity of hydrogen atom H29 is characterized by purple color which indicates that at this location electron are the most tightly bound. Hydrogen atom H29 and oxygen atom O27 are seen as reaction centers by MEP surface as well. One intra-molecular non-covalent interaction has been detected in the case of title molecule and it is located between atoms H29 and O26.

Besides ALIE surface, further insight into the local reactivity properties of investigated molecule can be obtained by Fukui functions. Fukui functions indicate how electron density changes with the addition or removal of the charge. If the charge is added it is useful to track where electron density increased. On the other side if the charge is removed than it is useful to track where electron density decreased. This is done by the so called f^+ and f^- functions, which are in Jaguar defined in the finite difference approximation as following:

$$f^+ = \frac{\left(\rho^{N+\delta}(r) - \rho^N(r)\right)}{\delta}, \quad (2)$$

$$f^- = \frac{\left(\rho^{N-\delta}(r) - \rho^N(r)\right)}{\delta}, \quad (3)$$

where N denotes the number of electrons in the reference state of the molecule and δ represents the fraction of electron, which is set to be 0.01 [74]. Values of Fukui f^+ and f^- functions have been mapped to electron density surface.

In case of f^+ function purple color is the positive color and it shows locations where electron density increases after the addition of charge. In case of f^- function red color is the negative color and it shows locations where electron density decreases after the removal of charge. Representative Fukui functions are presented in Fig.3. Results presented in Fig.3a indicate that with the addition of charge, electron density increases in the near vicinity of the carbon atoms C13, C19 and C4 and also in the case of nitrogen atom N25, and sulfur atom S28. Beside these atoms, possible reaction centers according to the Fukui f^- function is carbon atom C10, as red color in Fig.3b indicates that in the near vicinity of this atom electron density decreases with the removal of charge.

4.10 Reactive properties based on autoxidation and hydrolysis

DFT calculations and molecular dynamics simulations can be very useful to investigate degradation properties with respect to two main mechanisms: autoxidation and hydrolysis. Information about the autoxidation can be obtained by calculation of BDEs, while

information about the influence of hydrolysis mechanism can be obtained by calculations of RDF after MD simulations.

Concerning the process of autoxidation, if the hydrogen abstraction at certain location is possible with proper BDE values, then autoxidation process can start there. The prerequisite for the autoxidation process is that peroxy radical of pharmaceutical can abstract hydrogen from another pharmaceutical molecule [75]. Concretely, if the BDE value for hydrogen abstraction from pharmaceutical molecule is within 87 kcal/mol to 92 kcal/mol, than its location can be considered as possible starting location for the autoxidation. Mentioned interval is consequence of the fact that all peroxy radicals have similar mentioned BDE values, practically independent of chemical surrounding [75, 76]. According to the study of Wright et al. [78] it can be stated that BDE values from 75 to 85kcal/mol are the ones for which the pharmaceutical molecules are the most sensitive towards autoxidation. Values lower than 70-75 kcal/mol, are not suitable for autoxidation process [75, 77]. BDEs of all single acyclic bonds of the title molecule have been calculated and presented in Fig.4.

According to the obtained results only one BDE value for the hydrogen abstraction can be considered as possibly appropriate for the process of the autoxidation. That is the bond denoted with number 9 and is referring to the abstraction of hydrogen atom belonging to OH group. The calculated BDE value in this case is around 88kcal/mol and is not indicating the highest sensitivity towards autoxidation. On the other side the lowest BDE value for some single acyclic bond was calculated in the case of bond denoted with number 13, connecting the oxygen atom with methyl group. Its BDE value is just 55.60kcal/mol and is suggesting that degradation could start here as this bond is the weakest to break.

After the analysis of the results based on the MD simulations it can be concluded that autoxidation is not likely to happen in the case hydrogen atom H29. Namely, RDF, $g(r)$, represents the probability of finding a particle in the distance r from another particle [78]. Sharp peak profile and short distance of RDF curve indicate significant interactions with water molecules, Fig.5.

According to the results presented in Fig.5 it can be seen that precisely the most pronounced interactions with water molecules has hydrogen atom H29, with peak distance shorter than 2 Å. This means that processes of hydrolysis and autoxidation could compete at this location and since BDE value for abstraction of this hydrogen atom is higher than 85kcal/mol, it can be concluded that autoxidation process is not likely to happen. On the other side, beside H29, oxygen atom O27 also has pronounced interactions with water, with peak g(r) value of almost 1.4. Other non-carbon atoms with significant RDF profiles are

atoms H16, O26 and S28. Carbon atoms with representative RDF profiles are C8, C15, C17 and C21. According to the RDF parameters the most important carbon atom is C21, belonging to the methyl group. Its peak distance is located at around 3.5Å, while peak g(r) value is almost 1.6, the highest of all atoms. This result indicate that hydrolysis could be important degradation mechanism in the case of title molecule because mentioned carbon atom C21 is involved in the bond denoted with number 13, which is the weakest bond of all, as shown by BDE values.

4.11 Molecular docking

Based on the structure of a compound, PASS (Prediction of Activity Spectra) [79] is an online tool which predicts different types of activities. PASS analysis of the title compound predicts activities given in the Table S6 (supporting material), aryl hydrocarbon receptor activity with probability to be active (Pa) value of 0.767. The benzothiazole derivatives have exhibited interesting biological activities and attracting continuing interest for further molecular exploration as useful anticancer agents [80, 81]. The literatures enhance the antitumor activity of aryl hydrocarbon receptor Fukasawa [82, 83]. Thus we choose aryl hydrocarbon receptor is used as target for docking study. High resolution crystal structure of aryl hydrocarbon receptor was downloaded from the RSCB protein data bank website with PDB ID: 4xt2 and all molecular docking calculations were performed on Auto Dock-Vina software [84]. The 3D crystal structure of aryl hydrocarbon receptor was obtained from RCSB Protein Data Bank and the protein was prepared for docking by removing the co-crystallized ligands, waters and co-factors. The Auto Dock Tools (ADT) graphical user interface was used to calculate Kollman charges and polar hydrogen's. The ligand was prepared for docking by minimizing its energy at B3LYP/6-311++G(d) (5D, 7F) level of theory and partial charges were calculated by Geistenger method. The active site of the enzyme was defined to include residues of the active site within the grid size of 40Å×40Å×40Å. The most popular algorithm, Lamarckian Genetic Algorithm (LGA) available in Autodock was employed for docking. The docking protocol was tested by extracting co-crystallized inhibitor from the protein and then docking the same. The docking protocol predicted the same conformation as was present in the crystal structure with RMSD value well within the reliable range of 2Å [85]. Amongst the docked conformations, one which binds well at the active site was analyzed for detailed interactions in Discovery Studio Visualizer 4.0 software. The ligand binds at the active site of the substrate by weak non-covalent interactions and these interactions are depicted in Fig.S8 (supporting material) and Fig.6. Amino acids Glu320, Thr243 forms H-bond with OH group, phenyl ring respectively.

Thr324 forms π-π stacked interaction with phenyl and thiazole rings. Leu239 shows π-alkyl interactions with phenyl ring. The docked ligand forms a stable complex with aryl hydrocarbon receptor (Fig.7) and got a binding affinity value of -6.7kcal/mol (Table 3). Thus the title compound can be a lead compound for developing new anti-tumor drug.

4.12 Antimicrobial studies

The title compound was screened against one bacterial culture *Escherchia coli* and four fungal cultures *viz., Aspergillus niger, Pencillum chrysogenum, Saccharomyces cerevisiae* and *Rhyzopus stolonifer*. The antimicrobial properties were determined by the standard disc diffusion method [86]. The viable bacterial cells were swabbed onto MHA plates and fungal spores onto RBA plates. The compounds were dissolved in chloroform to a final concentration of 0.1%. The petri-plates were incubated for 24 h for bacterial cultures and 76 h for fungal cultures. The activity of the compounds was counted by measuring diameter of the inhibition zone in millimeters. Test substances which produce a zone of inhibition of 9 mm diameters or more are regarded as positive, *i.e.* having constructive antimicrobial activity, while in those cases where the diameter is below 9 mm, the bacteria are resistant to the sample tested and the sample is said to have no antimicrobial activity. The compound exhibits wide spectrum of activity against *Escherchia coli* with an inhibition zone of 34mm. Also it have inhibition zone against *Rhyzopus stolonifer* (10mm), *Saccharomyces cerevisiae* (8mm) and *Pencillum chrysogenum* (3mm) and no inhibition zone against *Aspergillus niger*.

5. Conclusion

A novel thiazole derivative, 2-(3-methoxy-4-hydroxyphenyl)benzothiazole is synthesized and single crystal XRD, FT-IR, FT-Raman, NMR and UV-Vis spectra are reported. The observed experimental and theoretical wave numbers were assigned using potential energy distribution. The calculated geometrical parameters are in agreement with the XRD values. The nonlinear optical properties are analyzed theoretically and the title compound is good object for further studies since the hyperpolarizability values are high. Beside carbon atoms of benzene rings, nitrogen atom N25 and sulfur atom S8 are recognized by ALIE surfaces as potentially vulnerable to electrophilic attacks. Atoms important from the aspect of local reactivity could also be carbon atoms C4, C13, C19 and nitrogen atom N25, as shown by Fukui functions. BDE values show that location of one hydrogen atom, H29, could be suitable for the process of autoxidation, but on the other side the same atom and adjacent atoms, O26 and O27, have the most pronounced interactions with water of all atoms of title

molecule, so processes of autoxidation and hydrolysis most likely compete at this location. It is also very important to emphasize the influence of water molecules to carbon atom C21. This atom is involved in the weakest bond, as shown by calculated BDE values, indicating that mechanism of hydrolysis could be very important for the degradation of title molecule. From molecular docking studies amino acids Glu320, Thr243 forms H-bond with OH group, phenyl ring respectively; Thr324 forms π-π stacked interaction with phenyl and thiazole rings; Leu239 shows π-alkyl interactions with phenyl ring. Antimicrobial studies of the compound show that there is a wide spectrum of activity against *Escherchia coli* with an inhibition zone of 34mm.

Acknowledgments

Part of this work has been performed thanks to the support received from Schrödinger Inc. Part of this study was conducted within the projects supported by the Ministry of Education, Science and Technological Development of Serbia, grant numbers OI 171039 and TR 34019 (project period 2016-2019/20). The authors are thankful to University of Antwerp for access to the University's CalcUA supercomputer cluster.

References

[1] X.H. Zhang, O.Y. Wong, Z.Q. Gao, C.S. Lee, H.L. Kwong, S.T. Lee, S.K. Wu, A new blue emitting benzothiazole derivative for organic electroluminescent devices, Mater. Sci. Eng.B, 85 (2001) 182-185.

[2] Y.I. Kim, S.K. Kang, Bis(2-amino-1,3-benzothiazole-N^3)dichloridozinc(II) ethanol hemisolvate, Acta Cryst. E68 (2012) m178-m179.

[3] H.-Y. Fu, X. Gao, G. Zhong, Z. Zhong, F. Xiao, B.Shao, Synthesis and electroluminescence properties of benzothiazole derivatives, J. Luminescence, 129 (2009) 1207-1214.

[4] V. Hrobarikova, P. Hrobarik, P. Gajdos, I. Fitilis, M. Fakis, P. Persephonis, P. Zahradnik, Benzothiazole based fluorophores of dono-π-acceptor-π-donor type displaying high two photon absorption, J. Org. Chem., 75 (2010) 3053-3068.

[5] G.K. Dutta, S. Guha, S. Patil, Synthesis of liquid crystalline benzothiazole based derivatives: A study of their optical and electrical properties, Org. Electron. 11 (2010) 1-9.

[6] S.K. Pal, T. Sahu, T. Misra, P.K. Mallick, M.N. P.-Row, T. Ganguly, Experimental investigation by laser flash photolysis to reveal the optical and electron donating

properties of benzothiazole derivatives and a theoretical approach by using time dependent density functional theory, J. Phys. Chem. A108 (2004) 10395-10404.

[7] W. Leng, Y. Zhou, Q. Xu, J. Liu, Synthesis and characterization of nonlinear optical side chain polyimides containing the benzothiazole chromophores, Macromolecules, 34 (2001) 4774-4779.

[8] E.M. Breitung, C.-F. Shu, R.J. Mc Mahon, Thiazole and thiophene analogues of donor-acceptor stilbenes: Molecular hyperpolarizabilities and structure property relationships, J. Am. Chem. Soc. 122(2000) 1154-1160.

[9] I. Hutchinson, M-S Chua, H.L. Browne, V. Trapani, T. D. Bradshaw, A.D. Westwell, M.F.G. Stevens, Antitumor benzothiazoles. 14. Synthesis and in vitro biological properties of fluorinated 2-(4-aminophenyl)benzothiazoles, J. Med. Chem. 44 (2001) 1446–1455.

[10] H. Bujdakova, T. Kuchta, E. Sidoova, A. Gvozdjakova, Anti Candida activity of four antifungal benzothiazoles, FEMS Microbiol. Lett. 112 (1993) 329-333.

[11] D. Cressier, C. Prouillac, P. Hernandez, C. Amourette, M .Diserbo, C Lion, G. Rima, Synthesis, antioxidant properties and radioprotective effects of new benzothiazoles and thiadiazoles, Bioorg. Med. Chem. 17 (2009) 5275-5284.

[12] W.P. Hu, Y.K. Chen, C.C. Liao, H.S. Yu, Y.M. Tsai, S.M. Huang, F.Y. Tsai, H.C. Shen, L.S. Chang, J.J Wang, Synthesis and biological evaluation of 2-(4-aminophenyl)benzothiazole derivative as photosensitizing agents, Bioorg. Med. Chem. 18 (2010) 6197-6207.

[13] M. Ono, S. Hayashi, H. Kimura, H. Kawashima, M. Nakayama, H. Saji, Push pull benzothiazole derivatives as probes for detecting β-amyloid plaques in Alsheimer's brains, Bioorg. Med. Chem. 17 (2009) 7002-7007.

[14] R. Minitha, Y.S. Mary, H.T. Varghese, C.Y. Panicker, R. Ravindran, K. Raju, V.M. Nair, FT-IR, FT-Raman and computational study of 1H-2,2-dimethyl-3H-phenothaizin-410H]-one, J. Mol. Struct. 985 (2011) 316-322.

[15] K.S. Resmi, K. Haruna, Y.S. Mary, C.Y. Panicker, T.A. Saleh, A.A. Al-Saadi, C. Van Alsenoy, Conformational, NBO, NLO, HOMO-LUMO, NMR, electronic spectral study and molecular docking study of N,N-dimethyl-3-(10H-phenothiazin-10-yl)-1-propanamine, J. Mol. Struct. 1122 (2016) 268-279.

[16] A. Golubović, B. Abramovic, M. Scepanovic, M. Grujic-Brojcin, S. Armakovic,

I. Veljkovic, B. Babic, Z. Dohcevic-Mitrovic, Z.V. Popovic, Improved efficiency of sol gel synthesized mesoporous anatase nano powdeers in photocatalytic degradation of metoprolol, Mater. Res. Bull. 48 (2013) 1363-1371.

[17] R. Ma, B. Wang, S. Lu, Y. Zhang, L. Yin, J. Huang, S. Deng, Y. Wang, G. Yu, Chacterization of pharmaceutically active compounds in dongting lake, china: Occurrence, chiral profiling and environmental risk, Sci. Total Environ. 557 (2016) 268-275.

[18] S.J. Armaković, S. Armakovic, N.L. Fincur, F. Sibul, D. Vione, J.P. Setrajcic, B. Abramovic, Influence of electron acceptors on the kinetics of metoprolol photocatalytic degradation in TiO_2 suspension. A combined experimental and theoreitcal study, RSC Advances, 5 (2015) 54589-54604.

[19] B. Abramović, S. Kler, D. Sojic, M. Lausevic, T. Radovic, D. Vione, Photocatalytic degradation of metoprolol tartrate in suspensions of two TiO2 based photocatalysts with different surface area, identification of inermediates and proposal of degradation pathways, J. Hazard. Mater. 198 (2011) 123-132.

[20] J.J. Molnar, J.R. Agbaba, B. Dalmacija, M.T. Klasnja, M.B. Dalmacija, M.M. Kragulj, A comparative study of the effects of ozonatoin and TiO_2 catalyzed ozonation on the selected chlorine disinfection by product precursor content and strucutre, Sci. Total Environ. 425 (2012) 169-175.

[21] J. Molnar, J. Agbaba, B. Dalmacija, M. Klasnja, M. Watson, M.Kragulj, Effects of ozonation and catalytic ozonation on the removal of natural organic matter from ground water, J. Environ. Eng., 138 (2012) 804-808.

[22] K. Deventer, G. Baele, P. Van Eenoo, O. Pozo, F. Delbeke, Stability of selected chlorinated thiazide diuretics, J. Pharm. Biomed. Anal. 49 (2009) 519-524.

[23] R. Munter, Advanced oxidation processes, current status and prospects, Proc. Estonian Acad. Sci. Chem, 50 (2001) 59-80.

[24] K.P. Madhusudanan, Direct Analysis in Real Time (DART) – A New Ionization Technique, Proceedings of 12th ISMAS-WS 2007, IT-9.

[25] P. Stenson, The crystal structure of 2-(o-hydroxyphenyl)benzothiazole, Acta Chem. Scand., 24 (1970) 3729-3738.

[26] U. Caruso, B. Panunzi, A. Roviello, M. Tingoli, A. Tuzi, Two aminobenzothiazole derivatives for Pd(II) and Zn(II) coordination, synthesis, characterization and solid state fluorescence, Inorg. Chem. Comm., 14 (2011) 46-48.

[27] E.D. Glendening, A.E. Reed, J.E. Carpenter, F. Weinhold, NBO version 3.1, TCI,

University of Wisconsin, Madison, 1998.

[28] A.D. Becke, Density functional exchange energy approximation with correct asymptotic behavior, Phys. Rev. A38 (1988) 3098-3100.

[29] Gaussian 09, Revision B.01, M.J. Frisch, G.W. Trucks, H.B. Schlegel, G.E. Scuseria, M.A. Robb, J.R. Cheeseman, G. Scalmani, V. Barone, B. Mennucci, G.A. Petersson, H. Nakatsuji, M. Caricato, X. Li, H.P. Hratchian, A.F. Izmaylov, J. Bloino, G. Zheng, J.L. Sonnenberg, M. Hada, M. Ehara, K. Toyota, R. Fukuda, J. Hasegawa, M. Ishida, T. Nakajima, Y. Honda, O. Kitao, H. Nakai, T. Vreven, J.A. Montgomery, Jr., J.E. Peralta, F. Ogliaro, M. Bearpark, J.J. Heyd, E. Brothers, K.N. Kudin, V.N. Staroverov, T. Keith, R. Kobayashi, J. Normand, K. Raghavachari, A. Rendell, J.C. Burant, S.S. Iyengar, J. Tomasi, M. Cossi, N. Rega, J.M. Millam, M. Klene, J.E. Knox, J.B. Cross, V. Bakken, C. Adamo, J. Jaramillo, R. Gomperts, R.E. Stratmann, O. Yazyev, A.J. Austin, R. Cammi, C. Pomelli, J.W. Ochterski, R.L. Martin, K. Morokuma, V.G. Zakrzewski, G.A. Voth, P. Salvador, J.J. Dannenberg, S. Dapprich, A.D. Daniels, O. Farkas, J.B. Foresman, J.V. Ortiz, J. Cioslowski, D.J. Fox, Gaussian, Inc., Wallingford CT, 2010.

[30] J.M.L. Martin, C. Van Alsenoy, GAR2PED, a Program to Obtain a Potential Energy Distribution from a Gaussian Archive Record, University of Antwerp, Belgium, 2007.

[31] R. Dennington, T. Keith, J. Millam, Gaussview, Version 5, Semichem Inc., Shawnee Mission, KS, 2009.

[32] J.B. Foresman, Pittsburg, PA, in: E. Frisch (Ed.), Exploring Chemistry with Electronic Structure Methods: a Guide to Using Gaussian, 1996.

[33] *Schrödinger Materials Science User Manual*. 2014, Schrödinger Press.

[34] A.D. Bochevarov, E. Harder, T.F. Hughes, J.R. Greenwood, D.A. Braden, D.M. Philipp, D. Rinaldo, M.D. Halls, J. Zhang, R.A. Friesner, Jaguar: A high performance quantum chemistry software program with strengths in life and materials sciences, Int. J. Quantum Chem. 113 (2013) 2110-2142.

[35] A.D. Becke, Density functional thermochemistry. III. The role of exact exchange, J. Chem. Phys. 98 (1993) 5648-5652.

[36] D. Shivakumar, J. Williams, Y. Wu, W. Damm, J. Shelley, W. Sherman, Prediction of absolute solvation free energies using molecular dynamics free energy perturbation and the OPLS force field, J. Chem.Theor. Comput. 6 (2010) 1509-1519.

[37] Z. Guo, U. Mohanty, J. Noehre, T.K. Sawyer, W. Sherman, G. Krilov, Probing the α-helical structural stability of stapled p53 peptides, molecular dynamics simulations and analysis, Chem. Biol. Drug Design, 75 (2010) 348-359.

[38] K.J. Bowers, E. Chow, H. Xu, R.O. Dror, M.P. Eashwood, B.A. Gregersen, J.L. Klepeis, I. Kolossvary, M.A. Moraes, F.D. Sacerdoti, *Scalable algorithms for molecular dynamics simulations on commodity clusters*. in *SC 2006 Conference, Proceedings of the ACM/IEEE*. 2006. IEEE.

[39] *Schrödinger Release 2015-4: Desmond Molecular Dynamics System, version 4.4, D. E. Shaw Research, New York, NY, 2015. Maestro-Desmond Interoperability Tools, version 4.4, Schrödinger, New York, NY, 2015.* 2015.

[40] J.L. Banks, H.S. Beard, Y. Cao, A.E. Cho, W. Damm, R. Farid, A.K. Felts, T.A. Halgren, D.T. Mainz, J.R. Maple, R. Murphy, D.M. Philipp, M.P. Repasky, L.Y. Zhang, B.J. Berne, R.A. Friesner, E. Galicchio, R.M. Levy, Integrated modeling program applied chemical theory (IMPACT), J. Comput. Chem. 26 (2005) 1752-1780.

[41] H.J. Berendsen, J.P. Postma, W.F. Van Gunsteren, J. Hermans, *Interaction models for water in relation to protein hydration*, in *Intermolecular forces*. 1981, Springer. p. 331-342.

[42] E.R. Johnson, S. Keinan, P. Mori-Sanchez, J. Contreras-Garcia, A.J. Cohen, W. Yang, Revealing non-covalent interactions, J. Am. Chem. Soc. 132 (2010) 6498-6506.

[43] J.S. Murray, J.M. Seminario, P. Politzer, P.Sjoberg, Average local ionization energies computed on the surfaces of some strained molecules, Int. J. Quantum Chem. 38 (1990) 645-653.

[44] K. Tamagawa, T. Iijima, M. Kimura, Molecular structure of benzene, J. Mol. Struct. 30 (1976) 243-253.

[45] Y.S. Mary, C.Y. Panicker, P.L. Anto, M. Sapnakumari, B. Narayana, B.K. Sarojini, Molecular structure, FT-IR, NBO, HOMO-LUMO, MEP and first order hyperpolarizability of (2E)-1-(2,4-dichlorophenyl)-3-(3,4,5-trimethoxyphenyl)pro-2-en-1-one by HF and density functional methods, Spectrochim. Acta 135 (2015) 81-92.

[46] Y.S. Mary, C.Y. Panicker, T.S. Yamuna, M.S. Siddegowda, H.S. Yathirajan, A.A. Al-Saadi, C. Van Alsenoy, Theoretical investigations on the molecular structure, vibrational spectral, HOMO-LUMO and NBO analysis of 9-[3-(dimethylamino)propyl]-2-trifluoro-mehtyl-9H-thioxanthen-9-ol, Spectrochim. Acta 132 (2014) 491-501.

[47] J.A. War, K.S. Resmi, Y.S. Mary, C.Y. Panicker, S.K. Srivastava, S. Makwane, Experimental IR, Laser Raman spectra and quantum chemical calculations of corrosion inhibitor 2-amino-5-ethyl-1,3,4-thiadiazole, Struct. Chem. Crystallo. Commun. 1 (2015) 1-6.

[48] N.P.G. Roeges, A Guide to the Complete Interpretation of Infrared Spectra of Organic Structures, John Wiley and Sons Inc., New York, 1994.

[49] B. Smith, Infrared Spectral Interpretation, A Systematic Approach, CRC Press, Washington, DC, 1999.

[50] R.M. Silverstein, G.C. Bassler, T.C. Morril, Spectrometric Identification of Organic Compounds, fifth ed., John Wiley and Sons Inc., Singapore, 1991.

[51] A.S. El-Azab, Y.S. Mary, C.Y. Panicker, A.A.M. Abdel-Aziz, M.A. El-Sherbeny, C. Van Alsenoy, DFT and experimental (FT-IR and FT-Raman) investigation of vibrational spectroscopy and molecular docking studies of 2-(4-oxo-3-phenethyl-3,4-dihydroquinazolin-2-ylthio)-N-(3,4,5-trimethoxyphenyl)acetamide, J. Mol. Struct. 1113 (2016) 133-145.

[52] N.B. Colthup, L.H. Daly, S.E. Wiberly, Introduction of Infrared and Raman Spectroscopy, Academic Press, New York, 1975.

[53] G. Varsanyi, Assignments of Vibrational Spectra of Seven Hundred Benzene Derivatives, Wiley, New York, 1974.

[54] K.B. Benzon, H.T. Varghese, C.Y. Panicker, K. Pradhan, B.K. Tiwary, A.K. Nanda, C. Van Alsenoy, Spectroscopic investigation (FT-IR and FT-Raman), vibrational assignments, HOMO-LUMO, NBO, MEP analysis and molecular docking study of 2-(4-hydroxyphenyl)4,5-dimethyl-1H-imidazole 3-oxide, Spectrochim. Acta 146 (2015) 307-322.

[55] A. Chandran, H.T. Varghese, C.Y. Panicker, C. Van Alsenoy, G. Rajendran, FT-IR and computational study of (E)-N-carbamimidoyl-4-((2-formyl benzylidene) amino)benzene sulfonamide, J. Mol. Struct. 1001 (2011) 29-35.

[56] C.Y. Panicker, H.T. Varghese, K.R. Ambujakshan, S. Mathew, S. Ganguli, A.K. Nanda, C. Van Alsenoy, Y.S. Mary, Ab initio and density functional theory studies on vibrational spectra of 3-{[(4-methoxyphenyl)methylene]amino}-2-phenylquinazolin-4(3H)-one, Eur. J. Chem. 1 (2010) 37-43.

[57] C.Y. Panicker, H.T. Varghese, K.R. Ambujakshan, S. Mathew, S. Ganguli, A.K. Nanda, C. Van Alsenoy YS.Mary, Vibrational spectra and computational study of 3-amino-2-phenyl quinazolin-4(3H)-one, J. Mol. Struct. 963 (2010) 137-144.

[58] Y.S. Mary, H.T. Varghese, C.Y. Panicker, T. Ertan, I. Yildiz, O.T. Arpaci Vibrational spectroscopic studies and ab initio calculations of 5-nitro-2-(p-fluorophenyl) benzoxazole, Spectrochim Acta 71 (2008) 566-571.

[59] C.Y. Panicker, H.T. Varghese, B. Narayana, K. Divya, B.K. Sarojini, J.A. War, C. Van Alsenoy, H.K. Fun, FT-IR, NBO, HOMO-LUMO, MEP analysis and molecular docking study of methyl N-({[2-(2-methoxyacetamido)-4-(phenylsulfanyl) phenyl]amino}[(methoxycarbonyl)imino]methyl)carbamate, Spectrochim. Acta 148 (2015) 29-42.

[60] K. Wolinski, J.F. Hinton, P. Pulay, Efficient implementation of the gauge independent atomic orbital method for NMR chemical shift calculations, J. Am. Chem. Soc. 112 (1990) 8251-8260.

[61] R. Sarma, B. Nath, A. Ghrilahre, J.B. Baruah, Study on changes in optical properties of phenylbenzothiazole derivatives on metal ion binding, Spectrochim. Acta, 77 (2010) 126-129.

[62] R.J. Abraham, M. Mobli, R.J. Smith, ^{1}H chemical shifts in NMR: Part 19. Carbonyl anisotropies and steric effects in aromatic aldehydes and ketones, Magn. Reson. Chem. 41(2003) 26-36.

[63] S. Ahmad, S. Mathew, P.K. Verma, Laser Raman and FT-infrared spectra of 3,5-dinitrobenzoic acid, Indian J. Pure Appl. Phys. 30 (1992) 764-765.

[64] Z. Liu, Y. Qu, M. Tan, H. Zhu, Acta Cryst. E60 (2004) o1310-o1311.

[65] Y.R. Shen, The Principles of Nonlinear Optics, Wiley, New York, 1984.

[66] C. Adant, M. Dupuis, J.L. Bredas, Ab inito study of the nonlinear optical properties of urea: Electron correlation and dispersion effects, Int. J. Quantum Chem. 56 (1995) 497-507.

[67] N. Choudhary, S. Bee, A. Gupta, P. Tandon, Comparative vibrational spectroscopic studies, HOMO-LUMO and NBO anlaysis of N-(phenyl)-2,2-dichloriacetamide, N-(2-chlorophenyl)-2,2-dichloroacetime and N-(4-chlorophenyl)-2,2-dichloroacetamide base on density functional theory, Comp. Theor. Chem. 1016 (2013) 8-21.

[68] N. Sinha, O. Prasad, V. Narayan, S.R. Shukla, Raman, FT-IR spectroscopic analysis and first order hyperpolarizability of 3-benzoyl-5-chlorouracidlby first principles, Mol. Simul. 37 (2011) 153-163.

[69] B. Kosar, C. Albayrak, Spectroscopic investigations and quantum chemical computational study of (E)-4-methoxy-2[(p-tolylimino)methylphenol Spectrochim. Acta 78 (2011) 160-167.

[70] G. Gece, The use of quantum chemical methods in corrosion inhibitor studies, Corros. Sci. 50 (2008) 2981-2992.

[71] K. Fukui, Role of frontier orbitals in chemical reactions, cience 218 (1982) 747-754.

[72] R.G. Parr. R.G. Pearson, Absolute hardness: companion parameter to absolute electronegativity, J. Am. Chem. Soc. 105 (1983) 7512-7516.

[73] P. Politzer, F. Abu-Awwad, J.S. Murray, Comparison of density functional theory and Hartree-Fock average local ionization, Int. J. Quantum Chem. 69 (1998) 607-613.

[74] A. Michalak, F. De Proft, P. Geerlings, R.F. Nalewajski, Fukui functions from the relaxed Kohn-Sham orbitals, J. Phys. Chem. 103A (1999) 762-771.

[75] T. Andersson, A. Broo, E. Evertsson, Prediction of drug candidates' sensitivity toward autoxidation: Computational estimation of C-H dissociation energies of carbon centered radicals, J. Pharm. Sci. 103 (2014) 1949-1955.

[76] Y.-R. Luo, *Handbook of bond dissociation energies in organic compounds*. 2002: CRC press.

[77] J.S. Wright, H. Shadnia, L.L. Chepelev, Stability of carbon centered radicals: Effect of functional groups on the energetic of addition of molecular oxygen, J. Comput. Chem. 30 (2009) 1016-1026.

[78] R.V. Vaz, J.R. Gomes, C.M. Silva, Molecular dynamics simulations of diffusion coefficients and structural propertie sof ketones in supercritical CO_2 at infinite dilution, J. Supercritic. Fluids, 107 (2016) 630-638.

[79] A. Lagunin, A. Stepanchikova, D. Filimonov, V. Poroikov, PASS: prediction of activity spectra for biologically active substances, Bioinformatics 16 (2000) 747-748.

[80] S.H.L. Kok, R. Gambari, C.H. Chui, M.C.W. Yuen, E. Lin, R.S.M. Wong, F.Y. Lau, G.Y M. Cheng, W.S. Lam, S.H. Chan, K.H. Lam, C.H. Cheng, P.B.S. Lai, M.W.Y. Yu, F. Cheung, J.C.O. Tang, A.S.C. Chan, Synthesis and anticancer activity of benzothiazole containing phthalimide on human carcinoma cell lines, Bioorg. Med. Chem. 16 (2008) 3626-3631.

[81] X.H. Shi, Z. Wang, Y. Xia, T.H. Ye, M. Deng, Y.Z. Xu, Y.Q. Wei, L.T. Yu, Synthesis and biological evaluation of novel benzothiazole-2-thiol derivatives as potential anticancer agents, Molecules 17 (2012) 3933-3944.

[82] K.Fukasawa, K. Kagaya, S.Maruyama, S.Kuroiwa, K.Masuda, Y.Kameyama, Y.Satoh, Y.Akatsu, A.Tomura, K.Nishikawa, S.Horie, Y. Ichikawa, A novel compound, NK150460, exhibits selective antitumor activity against breast cancer cell

lines through activation of aryl hydrocarbon receptor, Mol. Cancer Ther. 14 (2015) 343-354.

[83] J.H. Shin, L. Zhang, O. Murillo-Sauca, J. Kim, H.E.K. Kohrt, J.D. Bui, J.B. Sunwoo, Modulation of natural killer cell antitumor activity by the aryl hydrocarbon receptor, Proc. Natl. Acad. Sci. 23 (2013) 12391-12396.

[84] O. Trott, A. J. Olson, AutoDock Vina: Improving the speed and accuracy of docking with a new scoring function, efficient optimization and multithreading, J. Comput. Chem. 31 (2010) 455-461.

[85] B. Kramer, M. Rarey, T. Lengauer, Evaluation of the FlexX incremental construction algorithm for protein ligand docking, PROTEINS: Struct. Funct. Genet. 37 (1999) 228-241.

[86] C.H. Collins, P.M. Lyne, *'Microbiological Methods'*, University Park Press, Baltimore, 1970.

Figure Captions

Fig.1 Optimized geometry of 2-(3-methoxy-4-hydroxyphenyl)benzothiazole

Fig.2 Representative ALIE surface of 2-(3-methoxy-4-hydroxyphenyl)benzothiazole molecule

Fig.3 Representative Fukui functions a) f^{+} and b) f^{-}

Fig.4 BDE* of all single acyclic bonds of 2-(3-methoxy-4-hydroxyphenyl)benzothiazole molecule: *BDE for hydrogen abstraction are given in red color, while BDE for the rest of the single acyclic bonds are given in blue color

Fig.5 RDFs of atoms with significant interactions with water

Fig.6 Interactive plot of ligand and receptor and the H-bond surface shown

Fig.7 Surface view of the docked ligand embedded in the catalytic site of aryl hydrocarbon receptor

Table 1

Calculated scaled wave numbers, observed IR, Raman bands and assignments

B3LYP/6-311++G(d) (5D, 7F)			IR	Raman	Assignments[a]
υ(cm^{-1})	IRI	RA	υ(cm^{-1})	υ(cm^{-1})	-
3587	126.11	167.86	-	-	υOH(100)
3098	4.48	21.79	3096	3097	υCHI(99)
3075	6.67	178.06	-	-	υCHI(69)
3072	19.75	277.53	-	-	υCHII(99)
3066	24.08	151.39	-	3063	υCHII(99)
3055	14.06	51.92	-	-	υCHI(37), υCHII(62)
3055	3.69	132.00	-	-	υCHI(62), υCHII(32)
3044	1.29	47.43	-	3038	υCHII(95)
3027	25.53	144.06	3002	3003	υCH_3(99)
2970	31.39	34.86	2972	2970	υCH_3(100)
2908	40.39	131.84	2920	2905	υCH_3(100)
1583	31.38	334.09	1585	1585	υPhI(61), δCHI(18)
1579	58.27	472.90	-	-	υPhI(48), υPhII(18)
1569	17.02	288.35	-	1565	υPhII(58), υPhI(17)
1537	5.00	65.66	1533	1532	υPhII(65), δCHII(18)
1499	86.04	1862.83	1490	-	υC=N(23), υCC(14), υPhI(16), δCHI(15)
1467	238.41	1485.61	-	1470	υC=N(56), υPhI(18)
1460	134.35	143.76	1458	-	δCH_3(81)
1450	10.67	13.88	-	-	δCH_3(97)
1437	15.92	4.94	-	-	δCH_3(66), υPhII(12)
1433	3.92	144.93	-	1434	δCHII(12), υPhII(41)
1412	34.28	398.25	1420	1420	δCHII(22), υPhII(47)
1406	117.57	392.80	-	-	υPhI(40), δCH_3(11), δCHI(14)
1359	54.15	9.76	1361	1362	δOH(45), υPhI(46)
1295	15.90	15.76	1293	1301	υPhII(75), δCHII(10)
1277	0.37	58.81	-	1278	δCHI(50), υCN(12), υPhII(19)

1261	159.47	0.33	-	-	υPhI(53), υCN(17), υPhII(14)
1248	260.09	209.09	1250	1246	υCO(13), δCHI(15), δCHII(46)
1229	107.81	37.25	-	-	υCO(44), δPhI(16), δOH(11)
1219	19.77	422.06	-	-	υCN(48), δCHII(14)
1185	71.91	12.73	1190	1190	δCH_3(49), δCHI(11)
1170	146.78	392.25	-	1168	δOH(11), δCHI(42), υCC(11), υPhI(15)
1144	16.79	25.87	-	-	υCO(36), δCH_3(13), δCHI(17)
1140	2.15	6.87	-	-	δCHII(68), υPhII(19)
1136	0.56	2.34	-	1132	δCH_3(93)
1108	41.26	23.14	1114	-	δCHI(41), υPhI(15)
1102	5.83	126.03	-	-	δCHII(45), υPhII(22)
1042	13.02	127.07	1044	1038	δCHII(39), υPhII(41)
1018	37.65	9.66	1015	1019	υCO(50), δPhI(19)
999	11.67	60.20	-	-	υPhII(20), γCHII(21), δPhIII(27)
979	22.78	2.76	973	-	δPhIII(36), υCO(12), υPhI(18)
930	0.01	0.04	931	-	γCHII(89)
897	2.08	0.06	896	-	γCHII(89)
895	1.08	0.57	896	-	γCHI(82), τPhI(10)
864	26.46	0.32	861	-	δPhII(25), δPhIII(19), τPhI(32)
858	23.50	0.08	855	-	γCHI(72), τPhI(13)
818	1.05	0.06	816	-	γCHII(90)
807	8.13	38.39	-	802	δPhI(36), υCO(14)
790	23.83	0.04	-	788	γCHI(71)
759	50.22	22.74	756	756	υCS(35), υPhI(24)
731	62.38	1.29	-	729	γCHII(44), υPhI(45)
708	0.55	0.85	710	710	τPhI(52), γCO(36)
694	19.71	0.30	696	-	τPhII(53), γCHII(34)
689	0.83	20.26	-	-	δPhII(44), υCS(16), υPhII(15)
660	51.92	2.86	665	658	υCS(40), δCC(23), δPhIII(13)
626	4.48	9.51	630	633	δPhII(21), δPhI(34), δPhIII(15)

624	7.34	2.00	-	-	γCC(50), τPhIII(18), τPhI(17)
569	4.41	0.11	572	-	τPhIII(18), τPhII(21), τPhI(21), γCC(15)
563	7.98	0.74	560	561	δPhII(31), δPhI(17), δCO(14), δPhIII(13)
533	7.66	5.35	533	534	δCO(47), δPhI(25)
514	0.44	0.06	512	-	τPhII(35), τPhIII(14), τCC(13), τPhI(13)
498	2.64	2.80	-	503	δPhI(33), δCO(21), δPhIII(17)
489	0.72	16.12	485	-	δPhIII(47), δPhII(17)
441	0.62	0.68	-	439	τPhI(48), γCO(41)
426	117.07	1.09	430	424	τOH(94)
417	8.90	0.45	415	-	τPhII(64), δPhII(21)
404	0.89	3.02	-	-	γCC(17), δCO(12), δPhII(22), δPhIII(18)
349	0.01	1.06	-	-	γCO(24), τPhII(24), τPhI(30), τPhIII(11)
342	1.76	1.92	-	-	δCO(47), δPhI(14), δPhII(17)
287	0.06	0.38	-	-	τPhI(20), τCH_3(20), τPhII(19), γCC(14), γCO(12)
276	3.35	1.15	-	274	δCO(51), δCC(22)
243	2.24	0.98	-	250	δPhI(29), δPhIII(34)
239	0.39	0.48	-	-	τCH_3(50), τPhI(12), δPhII(15)
185	1.09	1.55	-	188	τPhI(22), τCH_3(13), δPhII(12), τPhI(27)
181	0.63	0.06	-	-	τPhIII(32), τPhII(40)
179	2.88	2.78	-	-	δCO(56), δCC(12)
124	0.04	2.43	-	-	τPhI(47), δPhII(17), τPhIII(15)
84	1.45	1.60	-	80	δCC(80)
74	5.38	0.54	-	-	τCO(70), τCH_3(25)
48	0.31	0.60	-	-	γCC(57), τPhI(22)

21	0.87	0.61	-	-	τCH_3(81)

[a]υ-stretching; δ-in-plane deformation; γ-out-of-plane deformation; τ-torsion; PhI-tri-substituted phenyl ring; PhII-1,2-substituted phenyl ring; PhIII-thiazole ring.

Table 2

Calculated electronic absorption spectrum of 2-(3-methoxy-4-hydroxyphenyl)benzothiazole using TD-DFT/ B3LYP/6-311++G(d) (5D, 7F)

Excitation -	CI expansion coefficient	Energy(eV) -	Wavelength (nm) calc	Oscillator Strength (f)
Excited State 1				
67→68	0.69121	3.8982	318.06	0.6348
Excited State 2				
66→68	0.64849	4.3170	287.20	0.0807
Excited State 3				
67→70	0.44576	5.3444	231.99	0.1341
Excited State 4				
66→70	0.47312	5.7582	215.32	0.1017
Excited State 5				
62→68	0.44513	6.1335	202.14	0.1396
Excited State 6				
64→69	0.34631	6.2531	198.28	0.0871
Excited State 7				
66→72	0.36635	6.6268	187.09	0.3019

Table 3

The binding affinity values of different poses of the title compound predicted by AutodockVina.

Mode	Affinity (kcal/mol)	Distance from best mode (Å)	
-	-	RMSD l.b.	RMSD u.b.
1	-6.7	0.000	0.000
2	-6.6	3.696	6.831
3	-6.2	12.672	14.192
4	-6.2	18.286	20.864
5	-6.1	3.605	7.934
6	-6.0	20.296	22.468
7	-5.9	9.664	12.121
8	-5.9	9.463	11.953
9	-4.9	21.409	23.518

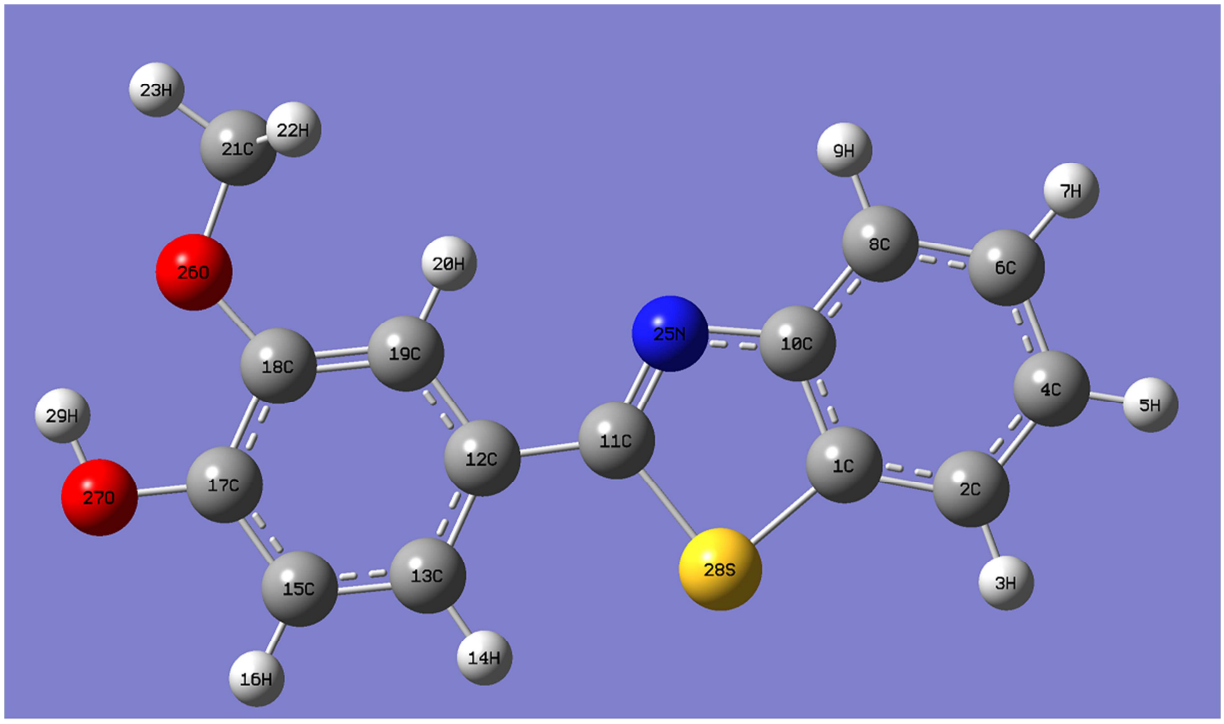

Fig.1 Optimized geometry of 2-(3-methoxy-4-hydroxyphenyl)benzothiazole

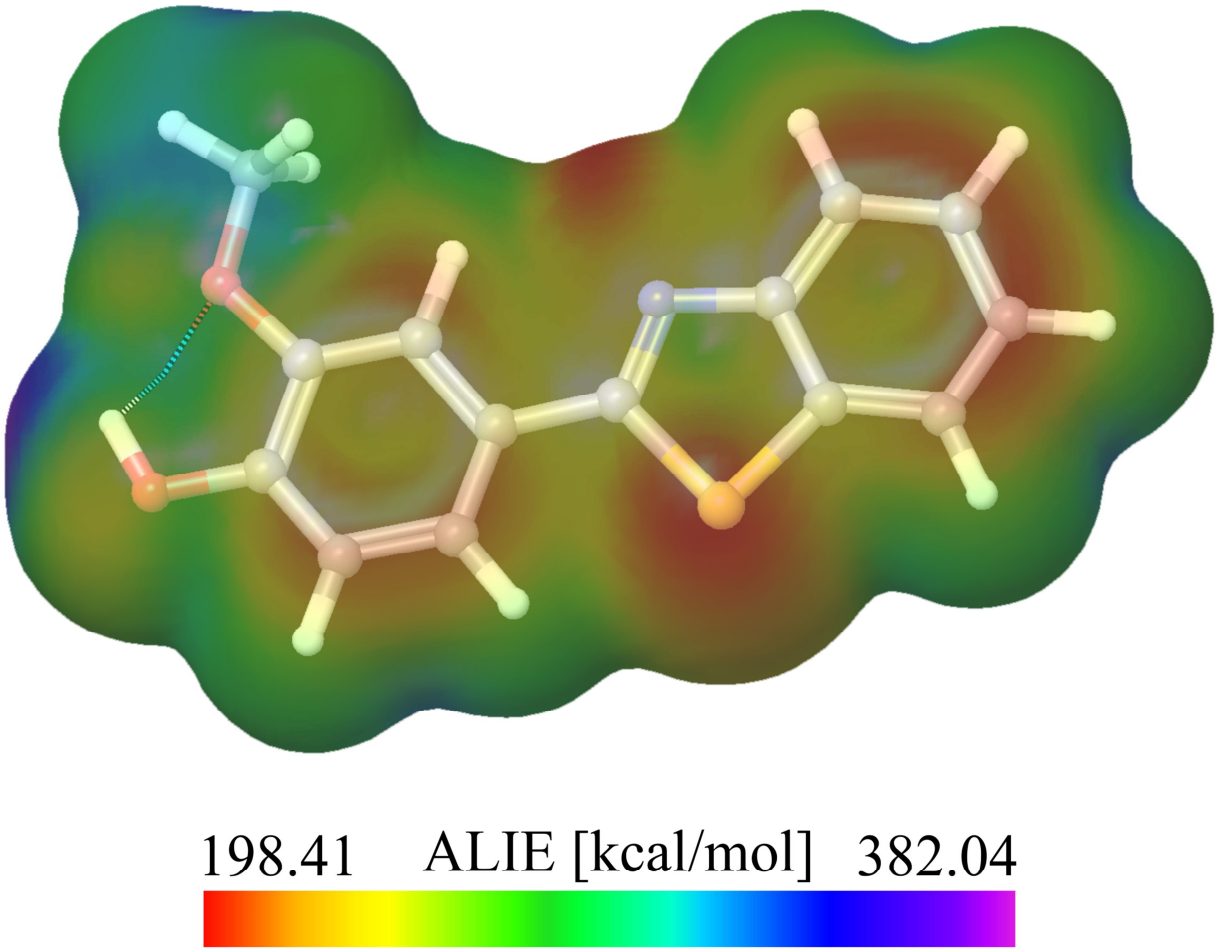

Fig.2 Representative ALIE surface of 2-(3-methoxy-4-hydroxyphenyl)benzothiazole molecule

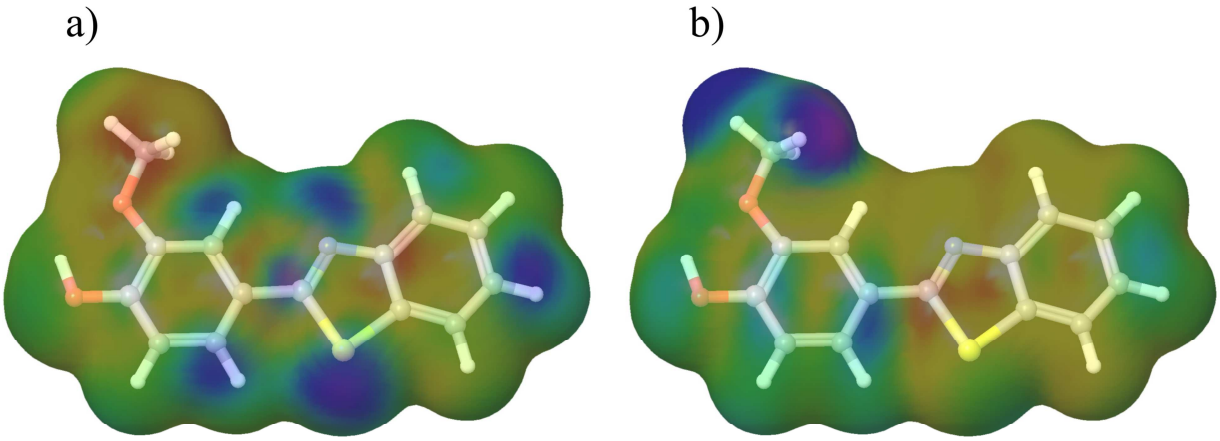

Fig.3 Representative Fukui functions a) f^+ and b) f^-

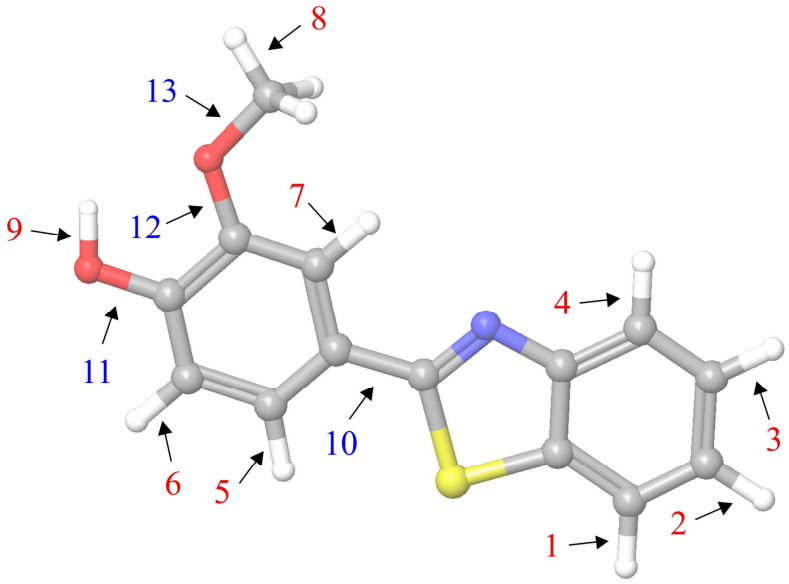

Bond	BDE [kcal/mol]
1	117.11
2	116.66
3	116.52
4	117.74
5	116.02
6	118.67
7	119.14
8	101.88
9	88.26
10	115.44
11	116.13
12	99.94
13	55.60

Fig.4 BDE* of all single acyclic bonds of 2-(3-methoxy-4-hydroxyphenyl)benzothiazole molecule: *BDE for hydrogen abstraction are given in red color, while BDE for the rest of the single acyclic bonds are given in blue color

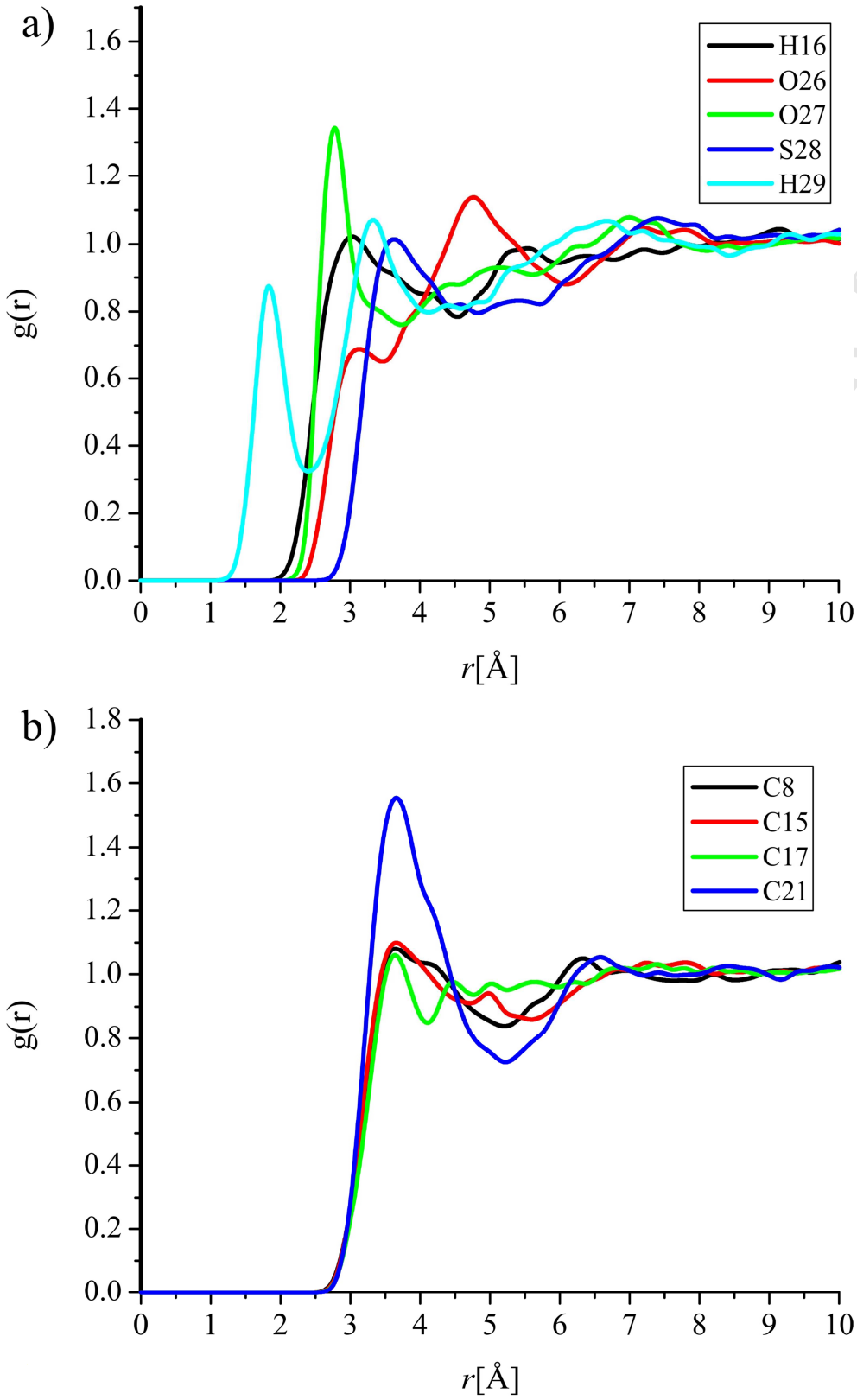

Fig.5 RDFs of atoms with significant interactions with water

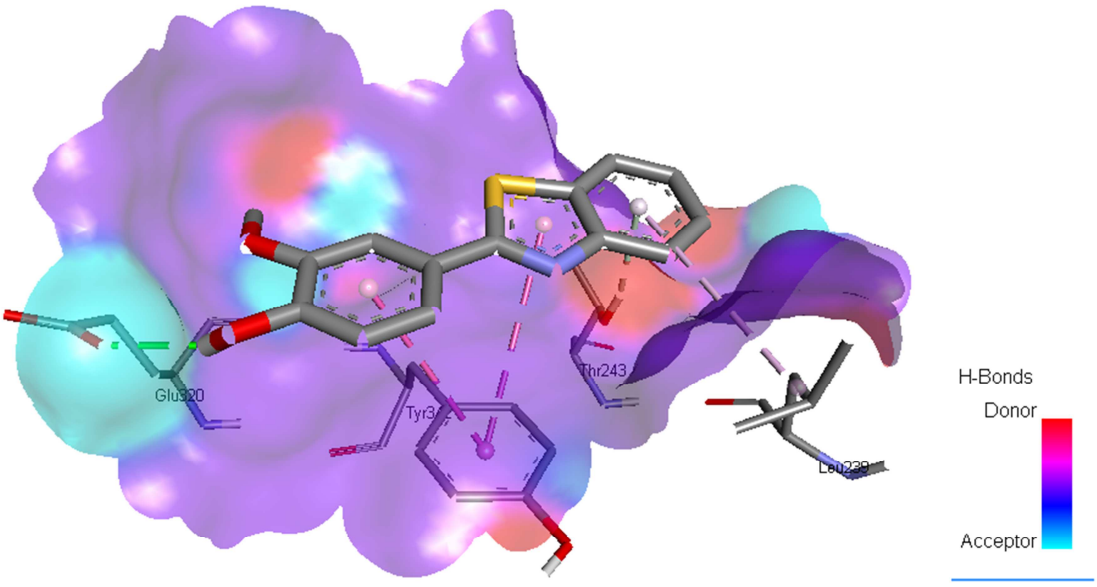

Fig.6 **Interactive plot of ligand and receptor and the H-bond surface shown**

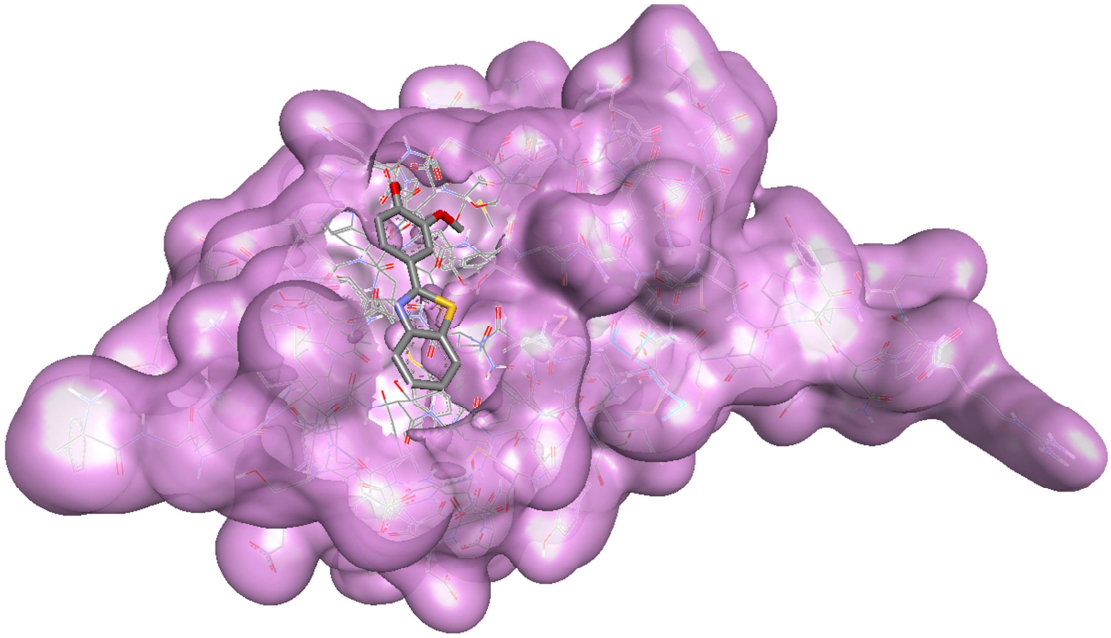

Fig.7 **Surface view of the docked ligand embedded in the catalytic site of aryl hydrocarbon receptor**

Highlights

- A novel thiazole derivative is synthesized and single crystal XRD is reported
- The recorded FT-IR and FT-Raman spectra were interpreted in detail with the aid of DFT and PED analysis
- Local reactivity properties are investigated by ALIE surfaces and Fukui functions
- Bond dissociation energies are calculated to predict the possible degradation properties
- Docking studies predict that the title compound can be a lead compound for developing anti-tumor drug